Journal of Materials Chemistry B

Accepted Manuscript

ROYAL SOCIETY OF CHEMISTRY

www.rsc.org/materialsB

Tunable Dual-stimuli Response of a Microgel Composite Consisting of Reduced Graphene Oxide Nanoparticles and Poly(*N*-isopropylacrylamide) Hydrogel Microsphere

Naiyan Lu,[a] Jiaojiao Liu,[a] Jingliang Li,[c] Zexin Zhang,[a] Yuyan Weng,[a] Bing Yuan,*[a] Kai Yang[a] and Yuqiang Ma*[b,a]

Received (in XXX, XXX) Xth XXXXXXXXX 200X, Accepted Xth XXXXXXXXX 200X
First published on the web Xth XXXXXXXXX 200X
DOI: 10.1039/b000000x

A type of photo- and thermo-responsive composite microspheres composed of reduced graphene oxide nanoparticles and poly(*N*-isopropylacrylamide) (rGO@pNIPAM) is successfully fabricated by a facile solution mixing method. Due to the high optical absorbance and thermal conduction of rGO , the composite microspheres are endowed the new property of photo-response, besides the intrinsic thermally sensitive property of pNIPAM. The new ability undoubtedly enlarges the scope of applications of the microgel spheres. Furthermore, through controlling the rGO content in the composite, the photo and thermo sensitivity of the composite can be effectively modulated. That is, with a lower rGO content (<=32% by weight), the composite microsphere performs only thermo induced changes, such as volume contraction (by ~45% in diameter) and drug release, when crossing the lower critical solution temperature of pNIPAM. With a higher rGO content (~47.5%), both temperature and light irradiation can trigger changes of the composite. However, when the rGO content increases to around 64.5%, the thermo responsibility of the composite disappears, and the sphere behaves only photo induced drug release. With a further increase in rGO content, the environmentally responsive ability of the microsphere vanishes.

1. Introduction

The ability of materials to response to dual or multiple stimuli is required for many advanced applications.[1–3] To this end, "multicomponent composites" are most attractive due to the diversity in their structure and the synergistic properties of the different components.[4,5] Recently, multi-responsive properties have been successfully achieved in polymeric hydrogels by incorporating inorganic nanomaterials.[6,7] The environmentally responsive changes of the obtained soft materials due to the hydrogel itself and/or the nanomaterials incorporated, endow these composites high importance in material and biomedical science applications, for example, in remote control,[8,9] targeted drug delivery,[10] controlled release[11–13] and so on.

Graphene, including reduced graphene oxide (rGO), has been proved to be a promising and unique inorganic nanocomponent for fabricating high-performance composites, due to its extraordinary mechanical, electronic and thermal properties, and relatively low cost.[14] There are also many efforts focusing on biological and medical applications of graphene because of its biocompatibility and unique conjugated structure.[15–17] Furthermore, it has been shown that graphene (or graphene oxide) is capable of converting optical energy into thermal energy efficiently.[11,12,16,18] For the application of graphene (oxide) in composites, previous studies mainly focused on its covalent functionalization, for example, to graft various polymers onto graphene sheets[10,12] or to polymerize polymer monomers directly in graphene oxide dispersed solutions.[8,9,19] Besides the considerable number of work done on graphene (oxide)-polymer composites, there is an increasing number of investigations made on graphene based hydrogel composites.[7–9,20–23]

As one of the most important environmentally responsive polymer, poly-*N*-isopropylacrylamide (pNIPAM) has attracted considerable attention. Thermal response is a key feature of pNIPAM. It undergoes a phase transition at a lower critical solution temperature (LCST) of around 32 ℃.[24,25] Below the LCST, pNIPAM is in a swollen state due to the hydrogen bonding with surrounding water molecules. Above the LCST, the hydrogen bonds break down leading to significant shrinkage of the materials such as a hydrogel it forms. Such a responsive behavior contributes to the applications of pNIPAM in many fields such as drug delivery.[9,26,27] However, the fabrication of pNIPAM composites with properties responsive to multiple stimuli has received less attention.[28]

In this study, we demonstrate a novel type of photo- and thermo-responsive microgel composite consisting of pNIPAM hydrogel sphere incorporated with rGO nanoparticles. This composite is facilely fabricated by mixing pre-synthesized rGO nanoparticle with pNIPAM microsphere dispersions with varying rGO contents. Besides the native thermo-sensitive character of pNIPAM, we took advantage of the high photo adsorption and thermal conduction abilities of rGO that decorated to the pNIPAM scaffold, to endow the composite with photo- and thermo-responsive phase transition and drug release properties. Furthermore, we show that with different rGO contents, the microgel composite demonstrates tunable photo- and thermo-dependent transition behaviors.

2. Experimental Section

Materials

Graphite powder was purchased from Sigma and used as received. The monomer *N*-isopropylacrylamide (NIPAM) was obtained from Acros. N,N′-Methylenebis(acrylamide) (MBA), Methacrylic acid (MAA) and potassium persulfate (KPS) were bought from Sigma. Calcein and the other chemicals used in the experiment (analytical reagent) were purchased from Shanghai Chemical Reagents Company and used without further purification. Distilled water (>18 MΩ·cm) was produced using a Millipore filter system.

Synthesis of rGO and pNIPAM microgel spheres

GO was first synthesized by a modified Hummers' method.[13,29] After oxidation, the product was washed copiously with distilled water, dialyzed for 3 days to remove any remaining ions, and sonicated 10 minutes to further exfoliate the GO sheets. To obtain rGO nanoparticles, hydrazine monohydrate was added into the solution.[11] The system was heated to 80 ℃ for 15 min, during which the color of the dispersion changed from yellow-brown to black and agglomeration occurred. After that, the supernatant was collected and sonicated for 30 minutes, which was then diluted to 0.2 mg mL^{-1} for further use.

The pNIPAM microgel particles were synthesized following Kwok's semi-batch precipitation polymerization method ($\varphi \sim 0.5$).[30] In brief, an amount of 0.9 g monomer NIPAM was dissolved in 55 mL distilled water and filtered to remove any solid impurities. The solution was purged with nitrogen gas to remove the dissolved oxygen, and stirred in a 40 ℃ water bath for 1 h. Then, 0.055 g KPS in 1 mL distilled water was added to initiate the polymerization. Two min later, 6 mL solution containing 0.3 g NIPAM, 0.032 g MBA, and 0.15 mL MAA was added at a rate of 5 mL per hour. When the reaction mixture started to turn opalescent, the temperature was ramped to 60 ℃ in 1 h. After all of the 6 mL comonomer solution was added, the reaction mixture was kept on being stirred for another 2 h.

Preparation of rGO@pNIPAM composite

The rGO@pNIPAM composite was prepared via a facile mixing method. A certain amount (from 15 to 1 μL, containing 7.5 to 0.5×10^8 pNIPAM spheres) of pNIPAM dispersion was added to 1,000 μL rGO dispersion to obtain a mixed solution with varying relative ratios of rGO to pNIPAM. The solutions, including the native rGO dispersion as a control, were diluted to a total volume of 1.015 mL, and gently stirred for 24 hours. The rGO@pNIPAM composite with different rGO contents was obtained during this process. The exact rGO content in the composite was determined through calculating the decrease of rGO quantity in the rGO solution after the addition of a certain amount of pNIPAM dispersion, which was obtained by Uv-vis absorbance test (*cf.* Electronic Supplementary Information, Section 2.1[†]). A weight percent of rGO in the rGO@pNIPAM composite (without water) was used to describe the rGO content in the composite.

Drug release test

Calcein was used as a model drug for the release test in the experiment.[27] A volume of 500 μL rGO@pNIPAM composite dispersion was transferred to a home-made sample cell for optical microscopic observation. After that, 200 μL saturated calcein solution was added into each cell. The composites were infiltrated with calcein immediately. Throughout the release period, the settings including the laser power and amplifier offset were maintained constant.[27,31]

Characterization

Powder X-ray diffraction (XRD) patterns were gathered on a Bruker D8-Advance diffractometer. Data from 5 to 40 ° were collected. AFM (Asylum Research, MFP-3D-SA) was used to confirm the complete exfoliation of GO and characterize the size and thickness distributions of rGO nanoparticles in water. The samples for AFM were prepared by dropping an aqueous GO or rGO dispersion onto a fresh silicon wafer, followed by drying under ambient conditions for 24 hours. SEM images were collected with a Raith Pioneer, a Hitachi S-3400N and a JEOL 7000F scanning electron microscope after freeze-drying the samples. Elemental analysis was done with the latter two pieces of equipment.

UV-vis absorbance spectrum was collected with a SHIMADZU UV3600 spectrometer. Fluorescence measurements were performed with a HORIBA Jobin Yvon FluoroMax-4 Fluorescence Spectrometer. Emission spectra of both the rGO nanoparticle and rGO@pNIPAM composite dispersions (under an excitation of 400 nm) were collected. All the spectroscopy tests were carried out at room temperature of 22 ℃.

The optical observation was performed on an inverted confocal fluorescence microscope (Zeiss, LSM 710) equipped with an oil immersion objective (100×). Calcein was excited at 488 nm and its fluorescence was collected in the green channel. The temperature of the system was modulated and maintained with the temperature control components from Zeiss. To observe the photo-response of rGO@pNIPAM, white light from a 103 W mercury lamp at 60% power intensity at full-waveband was irradiated on the particle under monitoring with an exposure area of 10×10 μm^2 for 10 minutes or a longer time as stated in the main text.

3. Results and discussion

3.1 Structural characteristics of rGO, pNIPAM microspheres, and rGO@pNIPAM composite

XRD profiles of graphene oxide before (GO) and after (rGO) reduction are shown in Fig. 1. For the GO sample, the prominent peak at 9.2 ° represents the lamellar structure of GO sheets, corresponding to an expanded inter-layer spacing of 9.6 Å, in comparison with the original graphite powder (~3.4 Å).[13] After reduction, the characteristic peak of GO was totally suppressed and instead, another diffraction peak was observed at around 33 ° referring to an inter-sheet spacing of 2.7 Å. This diffraction peak strongly suggests the significant loss of the functional groups (i.e. hydroxyl and epoxy) bound onto the basal plane of GO during reduction. Due to the

removal of functional groups from the GO sheets, the rGO sheets aggregated in the solution. Accordingly, the thickness increased from ~1 nm to 4–8 nm, according to AFM characterization (Fig. 2). Furthermore, the size of the rGO nanoparticles was reduced to 60–210 nm (mostly around 70 and 150 nm, with a mean of ~140 nm) in lateral width, as determined by both AFM and dynamic light scattering experiment (Fig. S1†) due to the sonication process, while that of the GO sheet is at a micrometer level (Fig. 2a).

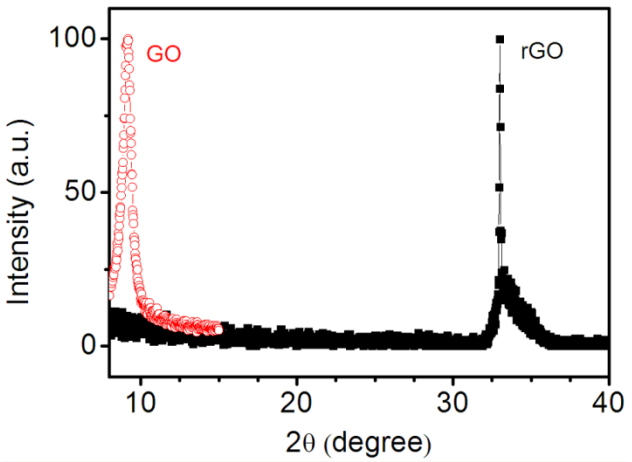

Fig.1 Normalized XRD profiles of as-made graphene oxide before (GO) and after reduction (rGO).

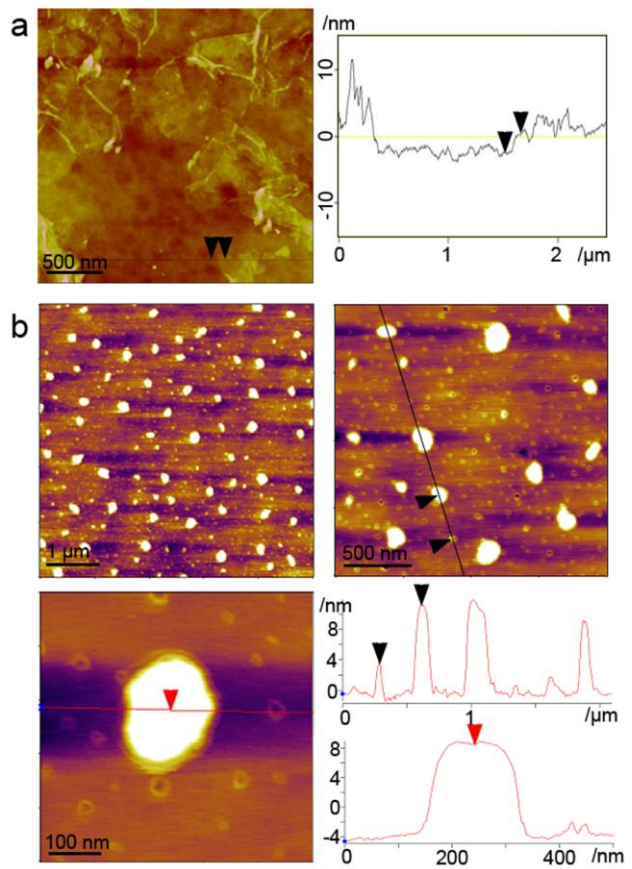

Fig. 2 AFM images with height profiles for GO (a) and rGO (b, at different magnifications).

The optical micrograph, SEM image, DLS and zeta potential profiles of the fabricated pNIPAM microgel spheres are given in the Supporting Information (Fig. S2†). The native pNIPAM microsphere shows a core-shell structure with a mean size of 2.7 ± 0.1 μm.[27,30,32] The spheres are positively charged with a zeta potential of ~14.6 mV.

During the fabrication process of rGO@pNIPAM composites, with the addition of pNIPAM solutions, obvious disturbance was observed in the rGO nanoparticle dispersions. The inset of Fig. 3 is a photo of the water dispersions of the composites with two typical rGO contents and the pristine rGO dispersion. The colorless and clear dispersion of rGO becomes cloudy upon the addition of pNIPAM (e.g. composite with 58% rGO) and even precipitation occurs (e.g. 87.5% rGO, *cf.* Fig. S3†). It suggests that the added pNIPAM microgel spheres might adsorb the originally well dispersed rGO nanoparticles, leading to aggregation and even precipitation. On the other hand, changes also happened to the spectral properties of the hybrid solution. The characteristic UV-vis absorbance peak at around 250 nm, originated from π-plasmon of carbon,[16,17] remains essentially the same. However, the absorption intensity decreases along with the increase in rGO loading in the composite microgels. This might be due to the adsorption of rGO nanoparticles into pNIPAM spheres that reduces the concentration of rGO dispersed in the solution. Fluorescence emission measurement in the visible range demonstrates the characteristic rGO peak at ~460 nm (with 400 nm excitation) for the rGO nanoparticle dispersions (Fig. 3b). No shift of the peak is observed upon the addition of pNIPAM, which indicates that no structural change (size or functional groups, *etc*) has occurred to the rGO nanoparticles.[12] This is completely different from the composites based on polymer anchored GO sheets.[12]

The adsorption of rGO nanoparticles to pNIPAM microgel was also confirmed by SEM. Fig. 4 shows SEM images of the composite microgel spheres (after freeze-drying) with different rGO contents, i.e., from the pristine pNIPAM to composite with 87.5% rGO. The structure of a native pNIPAM microgel sphere is core-shell alike with a rough surface of condensed pNIPAM polymer chains.[27,33] In strong contrast, the surface of the composite particles becomes much smoother and displays a lamellar morphology under high magnifications, especially for the samples with higher rGO/pNIPAM ratios (Fig. 4b–d). Such a lamellar structure is in consistence with that of the self-assembled supported rGO film.[13] Furthermore, the sizes of the freeze-dried composites under SEM, from 0, 32%, 70% to 87.5% rGO, are determined to be 1.2±0.1, 2.3±0.1, 3.0±0.2, and 3.5±0.2 μm, respectively (Fig. S4†). Such an increase in diameter corresponds to the significant increase in the content of rGO decorated to the pNIPAM microgel scaffold, in which the rGO nanoparticles work as cover and/or fillings to put up the size of the freeze-dried microgel samples. This increase in rGO content of the composites was further confirmed by elemental analysis. With the increase of rGO content, the elemental percentage of oxygen decreases while that of carbon increases (Fig. S5†).

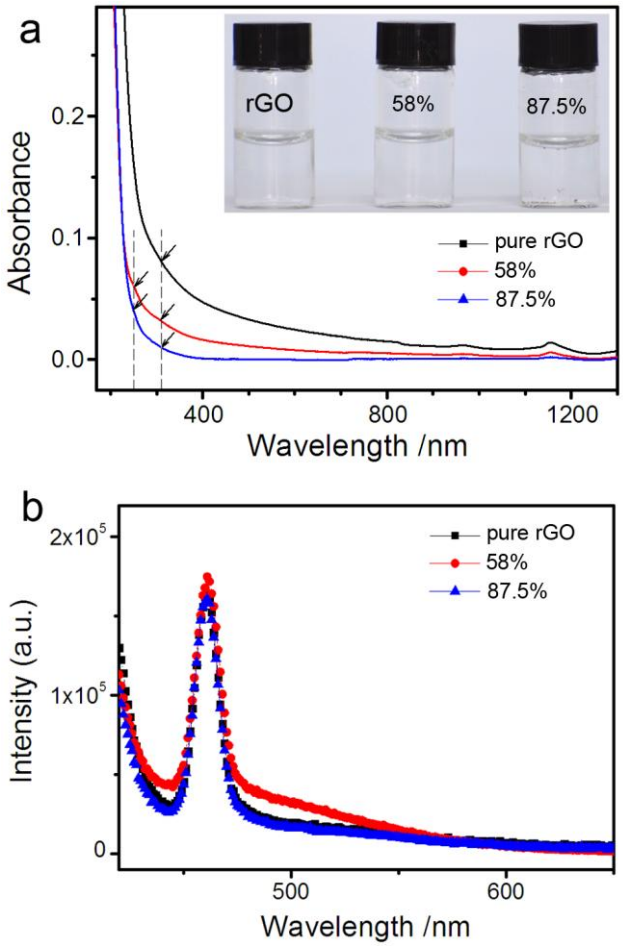

Fig. 3 UV–vis absorbance (a) and fluorescence (b) spectra of pristine rGO and composite (containing 58% or 87.5% rGO content) solutions. Inset: digital photograph of them. Black arrows point out the position of the absorbance peaks.

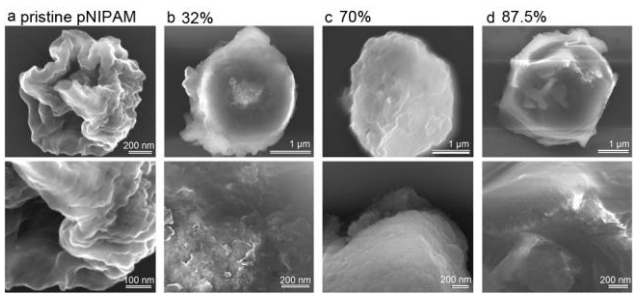

Fig. 4 SEM images of the freeze-dried composite samples containing different rGO contents, i.e. 0, 32%, 70% and 87.5%. The images in the bottom row are enlargements of the top ones.

Fig. 5 summarizes the effects of the rGO content on the morphology and size of the composite microgel spheres under optical microscope observations. (The size data here was obtained through calculating the size distribution of five model samples under observation and from three repeated experiments, which was further confirmed by DLS tests (ESI, Fig. S6†).) With the increase of rGO content from 0 to 87.5%, the composites become smaller and more distinguishable (Fig. 5-insets). This means that an increase in rGO content leads to a stronger contraction and a higher density of the composites. Furthermore, the changes in the shell of the composite are more remarkable in comparison with the core region, indicating that more rGO nanoparticles were incorporated into the shell layer of the pNIPAM microsphere, in contrast with the core region of it. The remarkable adsorption of rGO to pNIPAM might be attributed to two types of interactions: One is the interaction between the aromatic plane of rGO and the hydrophobic segments of pNIPAM polymer chains; the other might be due to the electrostatic interaction between the oppositely charged rGO and pNIPAM (Fig. S2-e†). The composite microspheres are stable over days.

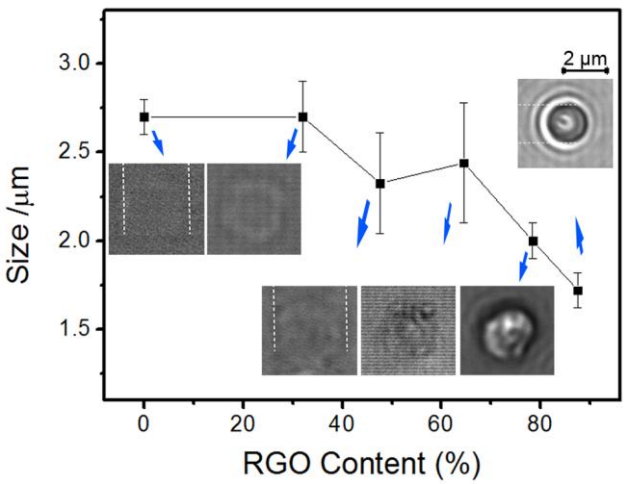

Fig. 5 RGO content dependence of the composite size obtained under optical microscope. Insets display the corresponding optical images (with the same magnification) of the composite spheres with increasing rGO contents.

3.2 Thermo- and photo-responsive behaviors

3.2.1 Thermo-dependent contraction and drug release (rGO content 0–32%)

In one of our previous work, we reported the thermo-stimulated contraction and drug release of pristine pNIPAM microspheres.[27] When the temperature was increased from 22 to 37 ℃ (crossing the LCST of pNIPAM), the calcein loaded in the pNIPAM microspheres was completely released within 10 minutes, along with the obvious volume contraction of the spheres (*e.g.* 45 ± 2% decrease in diameter, Fig. 6; Here, confocal image of a single typical sample is generally shown as an example.) After release, the final fluorescence intensity of calcein in the spheres was even lower than that of the bulk solution (*cf.* ESI, Section S2.2†). However, upon photo irradiation, no obvious influence was observed on either the pNIPAM microspheres or the loaded calcein, even after a longer exposure of 30 minutes (not shown).

For the composite microspheres with a small rGO content (e.g. 32%), similar results were obtained. Fig. 7 shows the response of 32% rGO composite under photic and thermal influences. Upon light irradiation for 10 minutes, no observable change in fluorescence intensity was observed. However, when the temperature of the system was increased from room temperature to 37 ℃, the composite sample changed from a bright sphere to a much smaller black particle

in 10 minutes. This means that particle contraction with calcein release have occurred. The size of the composite decreased by ~45%.

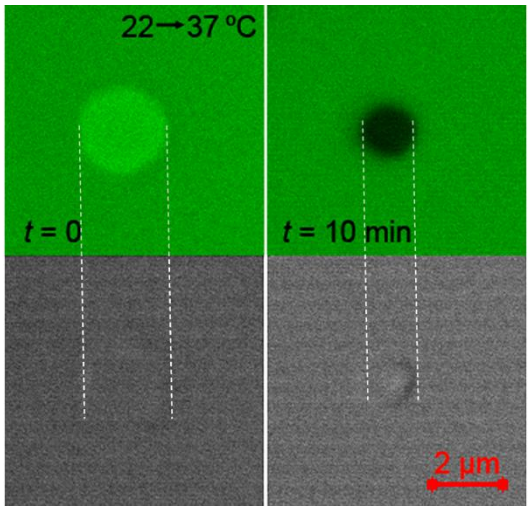

Fig. 6 Temperature-triggered contraction and release of a calcein-loaded pNIPAM microsphere (without rGO incorporation) after being incubated at 37 ℃ for 10 minutes. The first row gives fluorescence images and the second row gives transmission images.

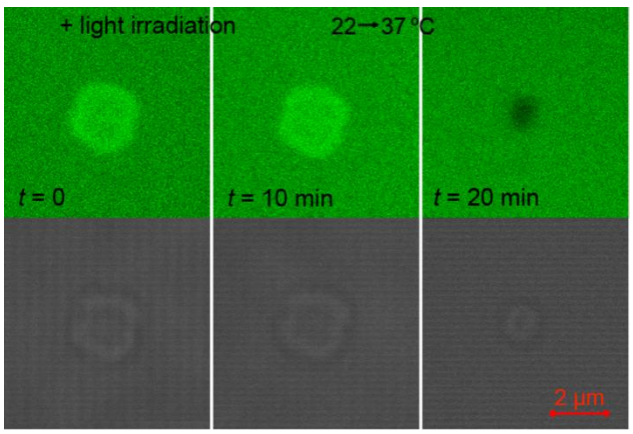

Fig. 7 Influences of a typical calcein-loaded rGO@pNIPAM composite microsphere (with 32% rGO) upon light irradiation and temperature changes (from 22 to 37 ℃) for 10 minutes, respectively.

3.2.2 Thermo- and light-dependent contraction and release (rGO content ~47.5%)

With a higher content of rGO, e.g. 47.5%, both thermo- and light-responsive properties of the composite microspheres were observed. Fig. 8a and b demonstrate the images of typical composite samples with 47.5% rGO content upon thermo and light irradiation treatments respectively. After being incubated at 37 ℃ for 10 minutes, both contraction and calcein release phenomena were observed for the composite microspheres. The size of the spheres decreased by ~45% (Fig. 8a). Similar phenomenon of calcein release was observed for the samples after 10 min light irradiation. However, only ~25% decrease in size was observed (Fig. 8b).

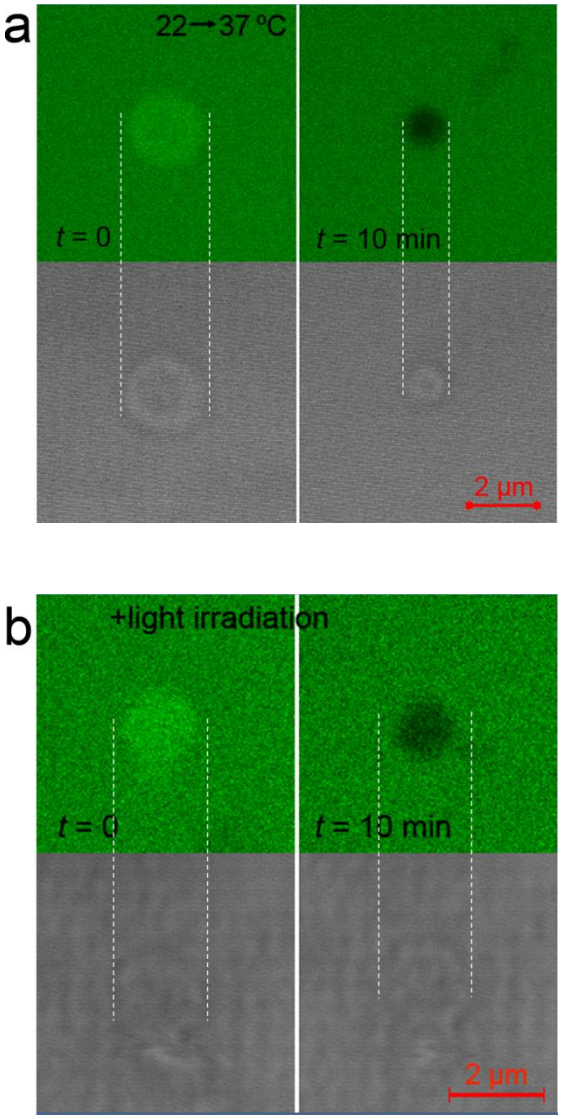

Fig. 8 Responses of typical composite samples with 47.5% rGO content upon thermal (a) or photic (b) treatment for 10 minutes, respectively.

3.2.3 Light-triggered release without contraction (rGO content ~64.5%)

When the rGO content within the rGO@pNIPAM composites increased to as high as 64.5%, no obvious influence was observed upon the thermal treatment (not shown). On the other hand, after being irradiated for 10 minutes, the sample under monitoring began dimming without any changes in size or morphology, indicating that calcein release from the composite had occurred (Fig. 9).

3.2.4 Composites independent of thermal or photic influence (>=78.5%)

For the rGO@pNIPAM composite microspheres with a rGO content around 78.5%, neither thermo nor light irradiation would lead to any change to the microspheres, even after a longer exposure of 30 minutes (Fig. 10). Furthermore, when the rGO content was increased to around 87.5%, the microsphere displays as a black sphere without any fluorescence (*cf.* ESI, Fig. S7†).

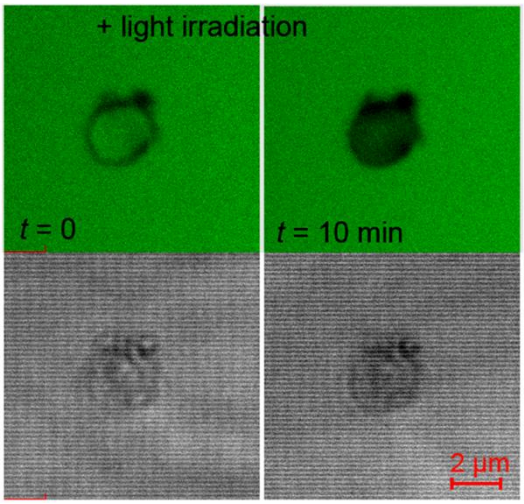

Fig. 9 Changes of a typical composite sample with 64.5% rGO content upon light irradiation for 10 minutes.

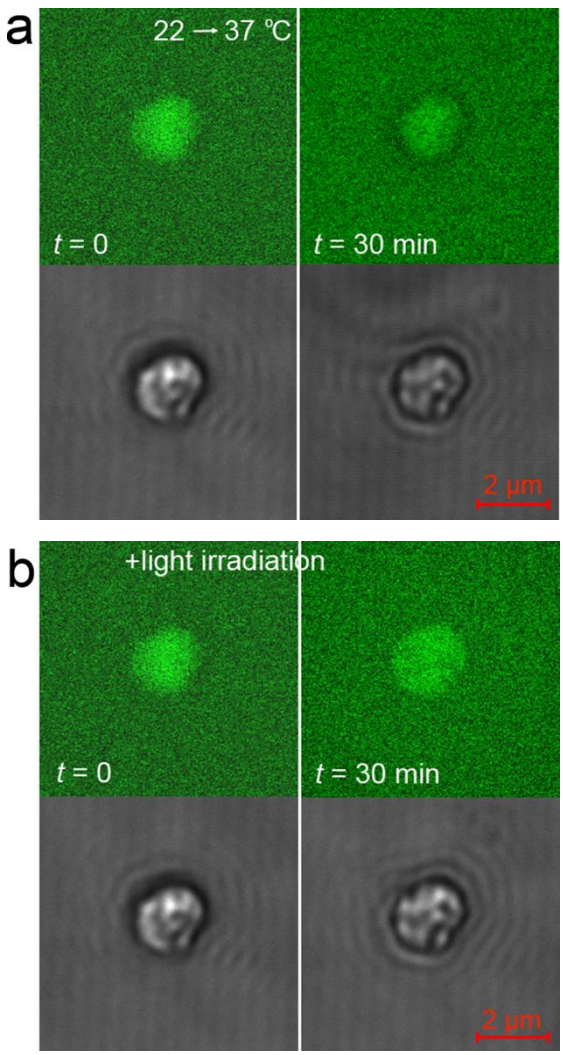

Fig. 10 No change is observed for the composite samples with 78.5% rGO content under either thermal (a) or photic (b) treatment, even after a longer time of 30 minutes.

Table 1. Thermo- and photo-dependent behaviors of rGO@pNIPAM composite microgel spheres with varying rGO contents.

rGO Content	Thermo-dependence	Photo-dependence
0	Contraction (~45%) + Release	×
32%	Contraction (~45%) + Release	×
47.5%	Contraction (~45%) + Release	Contraction (~28%) + Release
64.5%	×	Only Release
78.5%	×	×
87.5%	--	--

×, no changes occurred. --, not available.

3.3 Discussion

The thermo- and photo-responsive behavior of rGO@pNIPAM composite microspheres with different rGO contents are summarized in Table 1. The rGO@pNIPAM composites with small rGO contents (<=47.5%) demonstrate both thermo-triggered contraction and calcein release. When the rGO content exceeds 47.5%, these phenomena disappear. On the other hand, photo-dependent calcein release occurs (47.5% and 64.5%), although with a smaller degree of contraction or even without contraction of the microspheres. When the rGO content increases to around 78.5%, the composite remains stable upon both thermo and light irradiation treatments, without any observable changes.

It is noted that when the temperature of the system increases above the LCST of pNIPAM, volume phase transition of pNIPAM occurs which breaks the hydrogen bonds and extrudes the water from the inside of the hydrogel, leading to the contraction of the microsphere.[24] Moreover, it has been reported that rGO nanoparticles can convert light energy into thermal energy effectively.[12] The heat produced from rGO would be transmitted throughout the system due to the favorable heat conduction property of rGO,[12] leading to the increase of temperature. These are the reasons why some rGO@pNIPAM composites show both thermo- and photo-responsive behaviors. Furthermore, in our experiment, the thermo and photo dependence of the composite microspheres can be modulated by simply controlling the rGO content. It is noted that the most notable difference between the influences of thermo and light-irradiation treatments to a composite microsphere lies in that, the thermo influence probably occurs from the outside to the inside of the microgel sphere gradually, while the temperature increase of a composite upon light irradiation mostly originates from the rGO nanoparticles in the sphere simultaneously. It can be detailed as follows. (1) For the composite with a lower rGO loading (<47.5%), the heat produced from rGO upon light irradiation is not sufficient to induce phase transition of the pNIPAM, neither would it disturb the volume transition of the composite sphere upon temperature changes. As a result, the composite takes on only thermo-dependent contraction behavior like a pristine pNIPAM sphere. (2) For the composite with a higher rGO content (e.g. 64.5%), when the environmental temperature increases, heat transmits from the outside of the sphere to the

inside, which firstly leads to the contraction of the surrounding layer of pNIPAM microgel sphere. Consequently the decorated rGO nanoparticles self-assemble into a cover which enwraps the inner region of the sphere and prevents the release of water and calcein from the inside of it. (Note that the phase transition and volume contraction time of pNIPAM is on the order of seconds.[24]) However, for the spheres under light irradiation, phase transition occurs to all the rGO-decorated pNIPAM polymers simultaneously. As a result, calcein release is still likely to occur. (3) With a much higher rGO content (~78.5%), there are so many rGO nanoparticles adsorbed to the shell region of the microgel sphere that the nanoparticles work as fillings to prevent the volume changes of the microgel sphere upon either photo or thermo influence. Another possibility is that the abundant rGO replaces the hydrogen bonded water molecules with electrostatic interaction and consequently breaks down the thermo-repulsive phase transition character of pNIPAM (*cf.* ESI, Fig. S8†). In brief, by controlling the rGO content within the rGO@pNIPAM composite microgel spheres, we can effectively modulate the thermo- and light-triggered contraction and calcein release behaviors of the spheres.

On the other hand, it is interesting to find that with the increase of rGO content, the fluorescence intensity distribution of a calcein loaded composite changes (*cf.* ESI, Fig. S9†). That is, from 0, 32%, to 47.5%, the fluorescence of the shell region of a composite looks brighter than that of the core region; however, from 64.5% to 78.5%, the fluorescence of the shell region becomes even dimmer than the core. For the 87.5% sample, neither the shell nor the core region of the composite could be distinguished with fluorescence at all (Fig. S7†). Concerning that the incorporated rGO prefer to locate in the shell region of the pNIPAM sphere compared to the core region (*cf.* Section 3.1), such changes in fluorescence distribution could be attributed to the fluorescence quenching of calcein by rGO. We tested the fluorescence emission of calcein in the absence and presence of rGO and observed that with the addition of rGO, complete fluorescence quenching of calcein occurred (*cf.* ESI, Fig. S10†). Fluorescence quenching of dyes using rGO has been generally used in sensing applications.[34–37]

Another deserving attentive problem is that the incorporation of inorganic rGO nanoparticles into pNIPAM microgel particles would probably lead to the increase in the LCST of pNIPAM (*cf.* ESI, Section S2.3†).[38] However, this has been outside this work and would not be further discussed here.

4. Conclusions

A novel type of thermo- and photo-responsive composite microspheres was fabricated with rGO nanoparticles and pNIPAM hydrogel spheres. The combination of rGO with pNIPAM hydrogel leads to excellent photothermal properties, where the phase transition of the composite mirogel sphere can be remotely controlled by heat and/or light exposure. Furthermore, through controlling the rGO content incorporated in the composite, the thermal and photic sensitivity of the microsphere can be modulated. With a lower rGO content (<=47.5% by weight), increasing the temperature above the LCST of pNIPAM leads to a size contraction of the composite microsphere by ~45% along with the release of the loaded calcein from the inside of it. However, with a higher rGO content (>=64.5%), the composite does not change upon changing the temperature anymore. On the other hand, the composite microgel spheres with less rGO incorporation (<47.5%) do not demonstrate photo-repulsive contraction or calcein release behavior, until the rGO content increases to be >=47.5%. For the composites with a much higher rGO content (>=78.5%), the environmentally responsive behaviors no longer exist. Such rGO@pNIPAM composite microgel spheres with controllable thermo- and photo-responsive abilities promise applications in the biomedical field, especially for controlled delivery and release of drugs.

Acknowledgements

This work was financially supported by the National Science Foundation of China (Nos. 91027040, 31061160496, 21106114, 11104192 and 21204058), the National Basic Research Program of China (No. 2012CB821500), and the Natural Science Foundation of Jiangsu Province of China (Nos. BK2012177 and BK20131194).

Notes and references

[a] *Center for Soft Condensed Matter Physics and Interdisciplinary Research, Soochow University, Suzhou, 215006, P. R. China. E-mail: yuanbing@suda.edu.cn*

[b] *National Laboratory of Solid State Microstructures and Department of Physics, Nanjing University, Nanjing, 210093, P. R. China. E-mail: myqiang@nju.edu.cn*

[c] *Institute for Frontier Materials, Deakin University, Waurn Ponds, Vic, 3216, Australia.*

† Electronic Supplementary Information (ESI) available: Supporting Images and related explanations as mentioned in the main text. See DOI: 10.1039/b000000x/

1 C. Yuan, K. Raghupathi, B. C. Popere, J. Ventura, L. Z. Dai, S. Thayumanavan, *Chem. Sci.*, 2013, DOI: 10.1039/C3SC52347K.
2 Z. Tang, H. Kang, Q. Wei, B. Guo, L. Zhang, D. Jia, *Carbon*, 2013, **64**, 487.
3 J. Zhuang, M. R. Gordon, J. Ventura, L. Li, S. Thayumanavan, *Chem. Soc. Rev.*, 2013, **42**, 7421.
4 B. Yuan, L. L. Xing, Y. D. Zhang, Y. Lu, Z. H. Mai, M. Li, *J. Am. Chem. Soc.*, 2007, **129**, 22332.
5 Y. Chujo, *Curr. Opin. Solid State Mater. Sci.*, 1996, **1**, 806.
6 K. Haraguchi, *Polym. J.*, 2011, **43**, 223.
7 J. Liu, G. Chen, M. Jiang, *Macromolecules*, 2011, **44**, 7682.
8 C.-W. Lo, D. Zhu, H. Jiang, *Soft Matter*, 2011, **7**, 5604.
9 C.-H. Zhu, L. Yang, P. Jun, J.-F. Chen, S.-H. Yu, *Adv. Funct. Mater.*, 2012, **22**, 4017.
10 K.Yang, L. Hu, X. Ma, S. Ye, L. Cheng, X. Shi, C. Li, Y. Li, Z. Liu, *Adv. Mater.*, 2012, **24**, 1868.
11 J. T. Robinson, S. M. Tabakman, Y. Liang, H. Wang, H. S. Casalongue, D. Vinh, H. Dai, *J. Am. Chem. Soc.*, 2011, **133**, 6825.
12 X. Sun, Z. Liu, K. Welsher, J. T. Robinson, A. Goodwin, S. zaric, H. Dai, *Nano Res.*, 2008, **1**, 203.
13 B. Yuan, T. Zhu, Z. Zhang, Z. Jiang, Y. Ma, *J. Mater. Chem.*, 2011, **21**, 3471.
14 A. K. Geim, K. S. Novoselov, *Nat. Mater.*, 2007, **6**, 183.
15 Y. Zhang, T. R. Nayak, H. Hong, W. Cai, *Nanoscale*, 2012, **4**, 3833.
16 K.Yang, L. Feng, X. Shi, Z. Liu, *Chem. Soc. Rev.*, 2013, **42**, 530.
17 J.-L. Li, B. Tang, B. Yuan, L. Sun, X.-G. Wang, *Biomaterials*, 2013, **34**, 9519.

18 J.-L. Li, H.-C. Bao, X.-L. Hou, L. Sun, X.-G. Wang, M. Gu, *Angew. Chem. Int. Edit.*, 2012, **51**, 1830.
19 J. Dong, J. Weng, L. Dai, *Carbon*, 2013, **52**, 326.
20 S. Chen, J.-J. Duan, Y.-H. Tang, S.-Z. Qiao, *Chem. Eur. J.*, 2013, **19**, 7118.
21 C.-Y. Hou, Q.-H. Zhang, Y.-G. Li, H.-Z. Wang, *Carbon*, 2012, **50**, 1959.
22 Q.-Y. Cheng, D. Zhou, Y. Gao, Q. Chen, Z. Zhang, B.-H. Han, *Langmuir*, 2012, **28**, 3005.
23 S.-Z. Zu, B.-H. Han, *J. Phys. Chem. C*, 2009, **113**, 13651.
24 K. Makino, J. Hiyoshi, H. Ohshima, *Colloid. Surface. B*, 2000, **19**, 197.
25 Y. Zhang, S. Furyk, D. E. Bergbreiter, P. S. Cremer, *J. Am. Chem. Soc.*, 2005, **127**, 14505.
26 Y. Pan, H. Bao, N. G. Sahoo, T. Wu, L. Li, *Adv. Funct. Mater.*, 2011, **21**, 2754.
27 N. Lu, K. Yang, J. Li, Y. Weng, B. Yuan, Y. Ma, *J. Phys. Chem. B*, 2013, **117**, 9677.
28 Q. Saleem, B. Liu, C. C. Gradinaru, P. M. Macdonald, *Biomacromolecules*, 2011, **12**, 2364.
29 W. S. Hummers, R. E. Offeman, *J. Am. Chem. Soc.*, 1958, **80**, 1339.
30 M.-H. Kwok, Z. Li, T. Ngai, *Langmuir*, 2013, **29**, 9581.
31 F. Ungaro, M. Biondi, I. d'Angelo, L. Indolfi, F. Quaglia, P. A. Netti, M. I. La Rotonda, *J. Control. Release*, 2006, **113**, 128.
32 Y.-J. Dou, J.-L. Li, B. Yuan, K. Yang, *Appl. Surf. Sci.*, 2014, **296**, 95.
33 J. Liu, N. Lu, J. Li, Y. Weng, B. Yuan, K. Yang, Y. Ma, *Langmuir*, 2013, **29**, 8039.
34 C.-H. Lu, H.-H. Yang, C.-L. Zhu, X. Chen, G.-N. Chen, *Angew. Chem. Int. Edit.*, 2009, **48**, 4785.
35 J. H. Jung, D. S. Cheon, F. Liu, K. B. Lee, T. S. Seo, *Angew. Chem. Int. Edit.*, 2010, **49**, 5708.
36 H. Jang, Y.-K. Kim, H.-M. Kwon, W.-S. Yeo, D.-E. Kim, D.-H. Min, *Angew. Chem. Int. Edit.*, 2010, **49**, 5703.
37 B. J. Hong, Z. An, O. C. Compton, S. T. Nguyen, *Small*, 2012, **8**, 2469.
38 J. Dong, J. Weng, L. Dai, *Carbon*, 2013, **52**, 326.